Phase Field-Based Incompressible Two-Component Liquid Flow Simulation

Hosseini, Babak Sayyid; Möller, Matthias

DOI
10.1007/978-3-030-30705-9_15

Publication date
2020

Document Version
Accepted author manuscript

Published in
Numerical Methods for Flows - FEF 2017 Selected Contributions

Phase field-based incompressible two-component liquid flow simulation

Babak S. Hosseini and Matthias Möller

Abstract In this work, we consider a Cahn–Hilliard phase field-based computational model for immiscible and incompressible two-component liquid flows with interfacial phenomena. This diffuse-interface complex-fluid model is given by the incompressible Navier–Stokes–Cahn–Hilliard (NSCH) equations. The coupling of the flow and phase field equations is given by an extra phase induced surface tension force term in the flow equations and a fluid induced transport term in the Cahn–Hilliard (CH) equations. Galerkin-based isogeometric finite element analysis is applied for space discretization of the coupled system in velocity–pressure–phase field–chemical potential formulation. For the approximation of the velocity and pressure fields, LBB compatible non-uniform rational B-spline spaces are used which can be regarded as smooth generalizations of Taylor–Hood pairs of finite element spaces. The one-step θ-scheme is used for the discretization in time. For the validation of the two-phase flow model, we present numerical results for the challenging Rayleigh-Taylor instability flow problem in two dimensions and compare them to reference results.

1 Introduction

Multiphase flows comprise flow of materials with different phases (i.e gas, liquid, etc.), or materials with different chemical properties in the same phase, such as oil and water. In two-phase flows, being the most common multiphase flow configuration involving two distinct fluids, the fluids are segregated by a very thin interfacial

Babak S. Hosseini
TU Dortmund, Institute of Applied Mathematics (LS III), Vogelpothsweg 87, 44227 Dortmund, Germany, e-mail: babak.hosseini@math.tu-dortmund.de

Matthias Möller
Delft University of Technology, Delft Institute of Applied Mathematics, Van Mourik Broekmanweg 6, 2628 XE Delft, The Netherlands e-mail: m.moller@tudelft.nl

region where surface tension effects and mass transfer due to chemical reactions may appear. Multiphase flows are ubiquitous in nature and industrial systems and are quite challenging from the point of view of mathematical modeling and simulation due to the complex physical interaction between the involved fluids including topological changes and the complexity of having to deal with unknown moving fluid-fluid interfaces. As for methodologies to address the moving interface problem, there are various methods such as volume-of-fluid, front tracking, immersed boundary, level-set and phase field methods (cf. [5, 8]).

In this work we use a phase field diffuse interface method based on the Cahn–Hilliard equation and apply Isogeometric Analysis for the discretization of the involved equations. Particularly for two-phase flows, Diffuse-interface models have gained a lot of attention due to their ability to easily handle moving contact lines and topological transitions without any need for reinitialization or advective stabilization. On a general note, diffuse interface models allow the modeling of interfacial forces as continuum forces with the effect that delta-function forces and discontinuities at the interface are smoothed by smearing them over thin yet numerically resolvable layers. The phase field method – also known as the diffuse interface model – is based on models of fluid free energy and offers a systematic physical approach by describing the interface in a physical rather than in a numerical sense. One principal advantage of diffuse interface models is their ability to describe topological transitions like droplet coalescence or break-up in a natural way. In the phase field framework, the interface is modeled by a function $\varphi(x,t)$ which represents the concentration of the fluids. The function $\varphi(x,t)$, also referred to as the order parameter, or the phase field, attains a distinct constant value in each phase and rapidly, but smoothly, changes in the interface region between the phases. For a binary fluid, a usual assumption is that φ takes values between -1 and 1, or 0 and 1. The relaxation of the order parameter is driven by local minimization of the fluid free energy subject to the phase field conservation. As a result, complex interface dynamics such as coalescence or segregation can be captured without any special procedures [1, 9].

The outline of this article is as follows: In Section 2 we briefly introduce the mathematical model used in this work. It serves as a basis for Section 3 that is dedicated to the presentation of the weak forms and discretization aspects of the mathematical model with Isogeometric Analysis. We present our numerical results in Section 4 and conclude the article with a short summary in Section 5.

2 Navier–Stokes–Cahn–Hilliard two-phase flow model

Let $\Omega = (\Omega_1 \cup \Omega_2) \subset \mathbb{R}^n$ be an arbitrary open domain, with $n = 2$ or 3 and let its boundary $\partial\Omega$ be sufficiently smooth (e.g. Lipschitz continuous). Moreover, let Γ denote the interface between the different fluids or phases occupying the subdomains Ω_1 and Ω_2 and let $\mathbf{n}$ be the outward $(\Omega_1 \to \Omega_2)$ unit normal at the interface. The NSCH variable density, variable viscosity incompressible two-phase flow model (1) is obtained by the extension of the Navier–Stokes equations with a surface

tension force term $\eta\nabla\varphi$, written in its potential form, and a fluid induced transport term $\mathbf{v}\cdot\nabla\varphi$ in the Cahn–Hilliard equations (1c + 1d).

$$\rho(\varphi)\left(\frac{\partial\mathbf{v}}{\partial t}+(\mathbf{v}\cdot\nabla)\mathbf{v}\right)-\nabla\cdot\sigma(\varphi)=\rho(\varphi)\mathbf{g}+\eta\nabla\varphi \text{ in } \Omega_T, \tag{1a}$$

$$\nabla\cdot\mathbf{v}=0 \qquad \text{in } \Omega_T, \tag{1b}$$

$$\frac{\partial\varphi}{\partial t}+\mathbf{v}\cdot\nabla\varphi-\nabla\cdot(m(\varphi)\nabla\eta)=0 \qquad \text{in } \Omega_T, \tag{1c}$$

$$\eta-\beta\frac{d\psi(\varphi)}{d\varphi}+\alpha\nabla^2\varphi=0 \qquad \text{in } \Omega_T, \tag{1d}$$

$$\varphi(\mathbf{x},0)=\varphi_0(\mathbf{x}),\quad \mathbf{v}(\mathbf{x},0)=\mathbf{v}_0(\mathbf{x}) \qquad \text{in } \Omega, \tag{1e}$$

$$\frac{\partial\varphi}{\partial\mathbf{n}}=\frac{\partial\eta}{\partial\mathbf{n}}=0,\quad \mathbf{v}=\mathbf{v}_D \qquad \text{on } (\partial\Omega_T)_D, \tag{1f}$$

$$\left(-p\mathbf{I}+\mu(\varphi)\left(\nabla\mathbf{v}+(\nabla\mathbf{v})^T\right)\right)\cdot\mathbf{n}=\mathbf{t} \qquad \text{on } (\partial\Omega_T)_N. \tag{1g}$$

Above, $\Omega_T=\Omega\times(0,T)$, $(\partial\Omega)_D$ is the Dirichlet part of the domain boundary, $\sigma(\varphi)=-p\mathbf{I}+\mu(\varphi)\left(\nabla\mathbf{v}+(\nabla\mathbf{v})^T\right)$ denotes the (variable viscosity) fluid Cauchy stress tensor, $\mathbf{t}$ is the prescribed traction force on the Neumann boundary $(\partial\Omega)_N$, $\mathbf{g}$ is the gravitational force field and p is the pressure variable acting as a Lagrange multiplier in the course of enforcing the incompressibility condition. This basically corresponds to the model presented by Ding et al. [2] which can be seen as a generalization of "Model H" [4, 6] for the case of different densities and viscosities. In contrast to "Model H", a surface tension force term in potential form $\eta\nabla\varphi$ has replaced the divergence of the phase induced stress tensor $-\hat{\sigma}\varepsilon(\nabla\varphi\otimes\nabla\varphi)$. The latter, that is, $-\hat{\sigma}\varepsilon\,\mathrm{div}(\nabla\varphi\otimes\nabla\varphi)$, represents the phase induced force. In equation (1d), α and β are functions of the surface energy density $\hat{\sigma}$ and the interfacial region thickness ε.

In the Cahn–Hilliard equations (1c + 1d), $\varphi\in[-1,1]$ is a measure of phase and it holds $\varphi(x)=1$ (respectively $\varphi(x)=-1$) if and only if fluid 1 (respectively fluid 2) is present at point x. η represents the chemical potential and the nonlinear functions $m(\varphi)$ and $\psi(\varphi)$ model the concentration dependent mobility and fluid components' immiscibility, respectively.

3 Variational formulation and discretization

We use Isogeometric Analysis for the approximation of the solution of the coupled equation system (1). Inspired by operator splitting techniques, it is solved in two consecutive stages in order to alleviate numerical treatment. More specifically, given a flow field $\mathbf{v}$, we first solve the phase field equations (1c + 1d) in order to update the phase φ and chemical potential information η. The second step eventually uses these information to compute the surface tension force and the phase dependent values of density $\rho(\varphi(\mathbf{x}))$ and viscosity $\mu(\varphi(\mathbf{x}))$ in the course of the solution of

the Navier–Stokes equations (1a + 1b). As time integrator for both systems, we use the one-step θ-scheme with $\theta = 1$ or $\theta = 0.5$ yielding the 1st order implicit Euler or 2nd order Crank-Nicolson scheme, respectively. For the approximation of the velocity and pressure functions in the Navier–Stokes equations, we use LBB-stable Taylor–Hood-like B-spline/NURBS[1] space pairs $\hat{\mathbf{V}}_h^{TH}/\hat{Q}_h^{TH}$ which are defined in the parametric spline domain $\hat{\Omega}$ as

$$\begin{aligned} \hat{\mathbf{V}}_h^{TH} &\equiv \hat{\mathbf{V}}_h^{TH}(\mathbf{p},\alpha) = \boldsymbol{\mathcal{N}}_{\alpha_1,\alpha_2}^{p_1+1,p_2+1} = \mathscr{N}_{\alpha_1,\alpha_2}^{p_1+1,p_2+1} \times \mathscr{N}_{\alpha_1,\alpha_2}^{p_1+1,p_2+1}, \\ \hat{Q}_h^{TH} &\equiv \hat{Q}_h^{TH}(\mathbf{p},\alpha) = \mathscr{N}_{\alpha_1,\alpha_2}^{p_1,p_2}. \end{aligned} \tag{2}$$

Above, $\mathscr{N}_{\alpha_1,\alpha_2}^{p_1+1,p_2+1}$ denotes a tensor product bivariate NURBS space of polynomial degrees p_i+1 and continuities α_i, $i = 1,2$, with respect to parametric spline domain directions ξ_i. We refer to Hosseini et al. [7] for a detailed description of the above spline spaces. In all performed computations we used a $\mathscr{C}^0$ $\boldsymbol{\mathcal{N}}_{0,0}^{2,2}/\mathscr{N}_{0,0}^{1,1}$ NURBS space pair for the approximation of the velocity and pressure functions. This corresponds to the Isogeometric counterpart of a Q_2Q_1 Taylor–Hood space which is well known from the finite element literature. The degree and continuity of the discrete spaces used for the approximation of the Navier–Stokes velocity and Cahn–Hilliard phase and chemical potential functions are set to be identical. In the sequel we picture the individual solution stages and outline the spatial and temporal discretization of the involved equations.

STEP 1 – CAHN–HILLIARD EQUATION:

For the treatment of the nonlinearity in the advective Cahn–Hilliard equation, we seek for the current approximation of the solution $u^k = (\varphi^k, \eta^k)$ small perturbations $\delta u = (\delta\varphi, \delta\eta)$, such that

$$\begin{aligned} \varphi^{k+1} &= \varphi^k + \delta\varphi, \\ \eta^{k+1} &= \eta^k + \delta\eta \end{aligned} \tag{3}$$

satisfy the nonlinear partial differential equations (1c + 1d). Under the premise that $\delta\varphi$ is sufficiently small, we linearize the nonlinear function $\psi'(\varphi)$ as:

$$\psi'(\varphi^{k+1}) = \psi'(\varphi^k) + \psi''(\varphi^k)\,\delta\varphi + \mathscr{O}((\delta\varphi)^2) \approx \psi'(\varphi^k) + \psi''(\varphi^k)\,\delta\varphi. \tag{4}$$

After the time discretization by the one-step θ-scheme, we arrive at

$$\begin{aligned} \frac{\varphi^{n+1}-\varphi^n}{\Delta t} &+ \theta\left((\mathbf{v}\cdot\nabla)\varphi^{n+1} - \nabla\cdot m\nabla\eta^{n+1}\right) \\ &+(1-\theta)\left((\mathbf{v}\cdot\nabla)\varphi^{n} - \nabla\cdot m\nabla\eta^{n}\right) = 0 \quad \text{in } \Omega_T, \\ \eta^{n+1} &- \beta\,\psi'(\varphi^{n+1}) + \alpha\nabla^2\varphi^{n+1} = 0 \quad \text{in } \Omega_T, \end{aligned} \tag{5}$$

where the boundary terms have not been displayed for the sake of lucidity. Above, in the spirit of Picard iteration, the nonlinear mobility function $m(\varphi)$ is evaluated

[1] Non-Uniform Rational B-splines (NURBS)

with respect to the already available values of the phase field, that is, φ^n. This linearization allows us to treat it as a constant which simplifies its numerical treatment.

The variational form of the problem reads: Find $\varphi(\mathbf{x},t)$ and $\eta(\mathbf{x},t) \in \mathscr{H}^1(\Omega) \times (0,T)$, such that $\forall q, v \in \mathscr{H}_0^1(\Omega)$ it holds:

$$\begin{aligned}
&\int_\Omega \frac{\varphi^{n+1}-\varphi^n}{\Delta t}\, q \,\mathrm{d}\mathbf{x} + \theta\left(\int_\Omega (\mathbf{v}\cdot\nabla)\varphi^{n+1}\, q + m\nabla\eta^{n+1}\cdot\nabla q \,\mathrm{d}\mathbf{x} - \int_{\partial\Omega} \mathbf{n}\cdot m\nabla\eta^{n+1}\, q\, ds\right) \\
&\qquad +(1-\theta)\left(\int_\Omega (\mathbf{v}\cdot\nabla)\varphi^{n}\, q + m\nabla\eta^{n}\cdot\nabla q \,\mathrm{d}\mathbf{x} - \int_{\partial\Omega} \mathbf{n}\cdot m\nabla\eta^{n}\, q\, ds\right) = 0, \\
&\int_\Omega \eta^{n+1}\, v \,\mathrm{d}\mathbf{x} - \int_\Omega \beta\, \frac{d\psi(\varphi^{n+1})}{d\varphi}\, v \,\mathrm{d}\mathbf{x} - \int_\Omega \alpha\nabla\varphi^{n+1}\cdot\nabla v \,\mathrm{d}\mathbf{x} + \int_{\partial\Omega} \mathbf{n}\cdot\alpha\nabla\varphi^{n+1}\, ds = 0.
\end{aligned} \tag{6}$$

The application of (3) and (4) on (6) yields:

$$\begin{aligned}
&\int_\Omega (\varphi^k + \delta\varphi - \varphi^n)\, q \,\mathrm{d}\mathbf{x} + \theta\Delta t \int_\Omega (\mathbf{v}\cdot\nabla)(\varphi^k+\delta\varphi)\, q + m\nabla(\eta^k+\delta\eta)\cdot\nabla q \,\mathrm{d}\mathbf{x} \\
&\qquad +(1-\theta)\Delta t \int_\Omega (\mathbf{v}\cdot\nabla)\varphi^n\, q + m\nabla\eta^n\cdot\nabla q \,\mathrm{d}\mathbf{x} = 0, \\
&\int_\Omega (\eta^k+\delta\eta)\, v \,\mathrm{d}\mathbf{x} - \int_\Omega \beta\, \left(\psi'(\varphi^k) + \psi''(\varphi^k)\,\delta\varphi\right) v \,\mathrm{d}\mathbf{x} - \int_\Omega \alpha\nabla(\varphi^k+\delta\varphi)\cdot\nabla v \,\mathrm{d}\mathbf{x} = 0.
\end{aligned} \tag{7}$$

In equation (7), the indices n and k refer to the solution from the last time step and the current Newton-iterate, respectively. $(\delta\varphi, \delta\eta)$ is associated with the Newton-update.

Gathering all terms with the unknowns $\delta\varphi$ and $\delta\eta$ on the left hand side, we obtain the following expressions

$$\begin{aligned}
&\int_\Omega \underbrace{\delta\varphi\, q}_{\mathbf{M}} + \theta\Delta t \left(\underbrace{(\mathbf{v}\cdot\nabla)\delta\varphi\, q}_{\mathbf{C}} + m\underbrace{\nabla\delta\eta\cdot\nabla q}_{\mathbf{D}}\right) \mathrm{d}\mathbf{x} = \\
&\int_\Omega -\underbrace{\varphi^k q}_{\mathbf{M}} - \theta\Delta t \left(\underbrace{(\mathbf{v}\cdot\nabla)\varphi^k q}_{\mathbf{C}} + m\underbrace{\nabla\eta^k\cdot\nabla q}_{\mathbf{D}}\right) \mathrm{d}\mathbf{x} \\
&+\int_\Omega \underbrace{\varphi^n q}_{\mathbf{M}} - (1-\theta)\Delta t \left(\underbrace{(\mathbf{v}\cdot\nabla)\varphi^n q}_{\mathbf{C}} + m\underbrace{\nabla\eta^n\cdot\nabla q}_{\mathbf{D}}\right) \mathrm{d}\mathbf{x}, \\
&\int_\Omega \underbrace{\delta\eta\, v}_{\mathbf{M}} \,\mathrm{d}\mathbf{x} - \int_\Omega \beta\, \underbrace{\psi''(\varphi^k)\,\delta\varphi\, v}_{\mathbf{N}} \,\mathrm{d}\mathbf{x} - \int_\Omega \alpha\, \underbrace{\nabla\delta\varphi\cdot\nabla v}_{\mathbf{D}} \,\mathrm{d}\mathbf{x} = \\
&-\int_\Omega \underbrace{\eta^k v}_{\mathbf{M}} \,\mathrm{d}\mathbf{x} + \int_\Omega \beta\, \underbrace{\psi'(\varphi^k)\, v}_{\mathbf{n}} \,\mathrm{d}\mathbf{x} + \int_\Omega \alpha\underbrace{\nabla\varphi^k\cdot\nabla v}_{\mathbf{D}} \,\mathrm{d}\mathbf{x}.
\end{aligned} \tag{8}$$

The corresponding discrete system for the Newton-iteration may now be written in matrix form as

$$\underbrace{\begin{matrix} q \\ v \end{matrix}\begin{pmatrix} \mathbf{M}+\theta\Delta t\mathbf{C} & \theta\Delta tm\mathbf{D} \\ -\alpha\mathbf{D}-\beta\mathbf{N} & \mathbf{M} \end{pmatrix}}_{\mathbf{J}}\begin{pmatrix} \delta\varphi \\ \delta\eta \end{pmatrix} = \underbrace{\begin{pmatrix} -\mathbf{M}-\theta\Delta t\mathbf{C} & -\theta\Delta tm\mathbf{D} \\ \alpha\mathbf{D} & -\mathbf{M} \end{pmatrix}\begin{pmatrix} \varphi^k \\ \eta^k \end{pmatrix}+\begin{pmatrix} \mathbf{0} \\ \beta\mathbf{n} \end{pmatrix}+\begin{pmatrix} \mathbf{M}-(1-\theta)\Delta t\mathbf{C} & -(1-\theta)\Delta tm\mathbf{D} \\ \mathbf{0} & \mathbf{0} \end{pmatrix}\begin{pmatrix} \varphi^n \\ \eta^n \end{pmatrix}}_{-\mathbf{F}} \tag{9}$$

and solved for δu in order to update the unknowns as $(\varphi^{k+1},\eta^{k+1}) = (\varphi^k,\eta^k) + (\delta\varphi^k,\delta\eta^k)$.

STEP 2 – NAVIER–STOKES EQUATIONS: This step involves the numerical approximation of the solution of the unsteady variable density and variable viscosity Navier–Stokes equations extended by a surface tension force term. The initial condition for the velocity field is required to satisfy $\nabla\cdot\mathbf{v}_0 = 0$. With $\mathbf{b}$ denoting the body force term, the variational formulation of the problems (1a + 1b) reads: Find $\mathbf{v}(\mathbf{x},t) \in \mathscr{H}_0^1(\Omega)\times(0,T)$ and $p(\mathbf{x},t) \in \mathscr{L}_2(\Omega)/\mathbb{R}\times(0,T)$, such that for all $(\mathbf{w},q) \in \mathscr{H}_0^1(\Omega)\times\mathscr{L}_2(\Omega)/\mathbb{R}$ it holds

$$\begin{cases} (\mathbf{w},\mathbf{v}_t) + a(\mathbf{w},\mathbf{v}) + c(\mathbf{v};\mathbf{w},\mathbf{v}) + b(\mathbf{w},p) = (\mathbf{w},\mathbf{b}) + (\mathbf{w},\mathbf{t})_{(\partial\Omega)_N}, \\ b(q,\mathbf{v}) = 0. \end{cases} \tag{10}$$

Replacement of the linear-, bilinear- and trilinear forms with their respective definitions and application of integration by parts yields

$$\begin{aligned} &\underbrace{\int_\Omega \rho(\varphi)\mathbf{w}\cdot\mathbf{v}_t\,\mathrm{d}\Omega}_{(\mathbf{w},\mathbf{v}_t)} + \underbrace{\int_\Omega \mu(\varphi)\nabla\mathbf{w} : \left(\nabla\mathbf{v}+(\nabla\mathbf{v})^T\right)\mathrm{d}\Omega}_{a(\mathbf{w},\mathbf{v})} + \underbrace{\int_\Omega \rho(\varphi)\mathbf{w}\cdot\mathbf{v}\cdot\nabla\mathbf{v}\,\mathrm{d}\Omega}_{c(\mathbf{v};\mathbf{w},\mathbf{v})} = \\ &\underbrace{\int_\Omega \nabla\cdot\mathbf{w}\,p\,\mathrm{d}\Omega}_{b(\mathbf{w},p)} - \underbrace{\int_\Omega q\nabla\cdot\mathbf{v}\,\mathrm{d}\Omega}_{b(q,\mathbf{v})} + \underbrace{\int_\Omega \rho(\varphi)\mathbf{w}\cdot\mathbf{b}+\mathbf{w}\cdot\eta\nabla\varphi\,\mathrm{d}\Omega}_{(\mathbf{w},\mathbf{b})} + \\ &\underbrace{\int_{(\partial\Omega)_N}\mu(\varphi)\,\mathbf{w}\cdot\left(\left(\nabla\mathbf{v}+(\nabla\mathbf{v})^T\right)\cdot\mathbf{n}\right)\mathrm{d}(\partial\Omega)_N - \int_{(\partial\Omega)_N}\mathbf{w}\cdot\mathbf{n}\,p\,\mathrm{d}(\partial\Omega)_N}_{(\mathbf{w},\mathbf{t})_{(\partial\Omega)_N}}. \end{aligned} \tag{11}$$

A downcast of the variational formulation (10) to the discrete level gives rise to the problem statement

$$\begin{cases} \text{Find } \mathbf{v}^h \in \mathscr{H}_0^1(\Omega)\cap\mathbf{V}_h^{TH}\times(0,T) \text{ and } p^h \in \mathscr{L}_2(\Omega)/\mathbb{R}\cap Q_h^{TH}\times(0,T), \text{such that} \\ \forall(\mathbf{w}^h,q^h) \in \mathscr{H}_0^1(\Omega)\cap\mathbf{V}_h^{TH}\times\mathscr{L}_2(\Omega)/\mathbb{R}\cap Q_h^{TH} \\ (\mathbf{w}^h,\mathbf{v}_t^h) + a(\mathbf{w}^h,\mathbf{v}^h) + c(\mathbf{v}^h;\mathbf{w}^h,\mathbf{v}^h) + b(\mathbf{w}^h,p^h) = (\mathbf{w}^h,\mathbf{b}^h) + (\mathbf{w}^h,\mathbf{t}^h)_{(\partial\Omega)_N} \\ b(q^h,\mathbf{v}^h) = 0, \end{cases} \tag{12}$$

with superscript h dubbing the mesh family index. Using Isogeometric Taylor-Hood finite elements and the one-step θ-scheme for the respective discretizations in space and time, we obtain the following discrete system

$$\underbrace{\begin{pmatrix} \frac{1}{\Delta t}\mathbf{M}(\varphi^{n+1}) + \theta(\mathbf{D}(\varphi^{n+1}) + \mathbf{C}(v^{n+1},\varphi^{n+1})) & \mathbf{G} \\ \mathbf{G}^T & \mathbf{0} \end{pmatrix}}_{\mathbf{S}_l} \underbrace{\begin{pmatrix} \mathbf{v}^{n+1} \\ \mathbf{p}^{n+1} \end{pmatrix}}_{\mathbf{u}^{n+1}} =$$
$$\underbrace{\begin{pmatrix} \frac{1}{\Delta t}\mathbf{M}(\varphi^{n}) - (1-\theta)(\mathbf{D}(\varphi^{n}) + \mathbf{C}(v^{n},\varphi^{n})) & \mathbf{0} \\ \mathbf{0} & \mathbf{0} \end{pmatrix}}_{\mathbf{S}_r} \underbrace{\begin{pmatrix} \mathbf{v}^{n} \\ \mathbf{p}^{n} \end{pmatrix}}_{\mathbf{u}^{n}} + \underbrace{\theta\,\mathbf{f}^{n+1}(\eta^{n+1},\varphi^{n+1})}_{\mathbf{b}^{n+1}} + \underbrace{(1-\theta)\mathbf{f}^{n}(\eta^{n},\varphi^{n})}_{\mathbf{b}^{n}}, \tag{13}$$

where $\mathbf{M}, \mathbf{D}, \mathbf{C}, \mathbf{G}$, and $\mathbf{G^T}$ denote the mass, rate of deformation, advection, gradient, and divergence matrices, respectively. The body and the surface tension force terms are discretized altogether into $\mathbf{f}$. For the treatment of the nonlinearity in the Navier–Stokes equations (1a + 1b), we use the Newton-iteration

$$\mathbf{J}(\mathbf{u}^k, \varphi^k)\,\delta\mathbf{u} = -\mathbf{F}(\mathbf{u}^k, \mathbf{u}^n, \eta^k, \eta^n, \varphi^k, \varphi^n), \tag{14a}$$
$$\mathbf{u}^{k+1} = \mathbf{u}^k + \delta\mathbf{u}, \tag{14b}$$

whose right-hand side is set to be the residual of equation (13), that is,

$$\mathbf{F}(\mathbf{u}^{n+1}, \mathbf{u}^n, \eta^{n+1}, \eta^n, \varphi^{n+1}, \varphi^n) = \mathbf{S}_l\,\mathbf{u}^{n+1} - \mathbf{S}_r\,\mathbf{u}^n - \mathbf{b}^{n+1} - \mathbf{b}^n. \tag{15}$$

For a detailed description of the setup of the Jacobian $\mathbf{J}$ in equation (14), we refer to [7]. The linear equation systems arising from the discretization of the Cahn–Hilliard and Navier–Stokes equations are solved with direct solvers. For the solution of corresponding 3D problems involving larger systems, iterative solvers are advisable.

4 Application to the Rayleigh-Taylor instability problem

The Rayleigh-Taylor instability is a two-phase instability which occurs whenever two fluids of different density are accelerated against each other. Any perturbation along the interface between a heavy fluid (F_H) on top of a lighter fluid (F_L), both subject to a gravitational field, gives rise to the phenomenon of Rayleigh-Taylor instability. The initial perturbations progress from an initial linear growth phase into a non-linear one, eventually developing "mushroom head" like structures moving upwards and thinning "spikes" falling downwards. Assuming negligible viscosity and surface tension, the instability is characterized by the density disparity, measured with the Atwood number $\mathscr{A} = (\rho_H - \rho_L)/(\rho_H + \rho_L)$. For the validation of our results, we will consider the works of Tryggvason [10] and Guermond et al. [3] as reference. The former investigated the initial growth and long-time evolution of the instability for incompressible and inviscid flows with zero surface tension at $\mathscr{A} = 0.5$. Guermond et al., on the other hand, studied this instability problem at the same Atwood number, however, taking viscous effects additionally into account.

The setup of the problem is described by a rectangular computational domain $[0,d] \times [0,4d]$, where an initial wavy interface segregates a heavier fluid in the upper domain part from a lighter fluid on the lower part. The initial interface is described by the function

$$y(x) = 2d + 0.1d\cos(2\pi x/d)$$

representing a planar interface superimposed by a perturbation of wave number $k = 1$ and amplitude $0.1d$. Note that setting the surface tension coefficient $\hat{\sigma}$ to 0, effectively downgrades the Cahn–Hilliard equations (1c + 1d) to a pure transport equation well known from the level-set context. This, in turn, implies to pass on both the physical benefits inherent to phase field models and to the automatic recreation of the smooth transition of the phase field in the interface region. In order to circumvent these issues, we chose to set the surface tension coefficient to the small, yet non-zero value 0.01. As for the remaining simulation parameters we set $d = 1, \rho_H = 3, \rho_L = 1, \mu_H = \mu_L = 0.0031316$ and $g = 9.80665$, giving rise to $\mathscr{A} = 0.5$ and $Re = \rho_H d^{3/2} g^{1/2}/\mu_H = 3000$. At the top and bottom boundaries we use the no-slip boundary condition, whereas the free slip boundary condition is imposed on the vertical walls. Figure 1 depicts our results for the temporal evolution of the interface computed in the time interval $[0, 1.5]$ with $\Delta t = 0.001, h = 2^{-7}, \varepsilon = 0.005$ and $D = 0.00004$. As anticipated, the heavier fluid on top starts to fall through the lighter fluid and gradually develops spikes which are subject to strong deformations. When it comes to the comparison of the vortex structure with the "inviscid" results of Tryggvason and the "viscous" results of Guermond et al., our viscous solution exhibits a satisfactory agreement with both, especially with the latter mentioned. Note that the data provided by the above references are computed with respect to individual scalings of the involved PDE variables in order to obtain nondimensional variables. Therefore, comparisons require the time scales of the respective simulations to be mapped to each other. Since, in contrast to the reference results, we did not perform any rescaling, our time t is mapped to Tryggvason's time $\tilde{t}$ via the relation $t = \sqrt{d/(\mathscr{A} g)}\,\tilde{t}$.

We continue the validation of our results with a quantitative analysis and conduct a comparison of the tip of the rising and falling fluids with the inviscid and viscous results provided by Tryggvason and Guermond et al., respectively. The results, depicted in Figure 2, are in good agreement with both references whose data have individually been translated along the y-axis to facilitate comparisons. The upper curve referring to the tip of the rising fluid shows a better correlation with the data provided by Tryggvason while our curve for the falling fluid seems to perfectly match the results of Guermond. As for space and time discretization, for the results depicted in Figure 2, Guermond uses $P_2 - P_1$ finite elements on a 49577 P_2 nodes mesh with a time step size $\Delta\tilde{t} = 5 \times 10^{-4}$. Tryggvason on the other hand uses a Lagrangian-Eulerian vortex method on a 64×128 grid. Our results depicted in Figures 1, 2 and 3, are obtained using a fully implicit time integration ($\theta = 1$) in combination with a space discretization based on a $\mathscr{C}^0$ $\boldsymbol{\mathcal{N}}^{2,2}_{0,0}/\mathscr{N}^{1,1}_{0,0}$ NURBS space pair for the approximation of the velocity and pressure functions. For mesh refinement levels $h \in \{2^{-5}, 2^{-6}, 2^{-7}\}$ the above choice of space discretization yields $\{(33410, 4257), (132354, 16705), (526850, 66177)\}$ (velocity, pressure) degrees of freedom, respectively. Note that with the above mentioned relation between t and $\tilde{t}$, our time step $\Delta t = 0.001$ is mapped to $\Delta\tilde{t} = 0.0022143$.

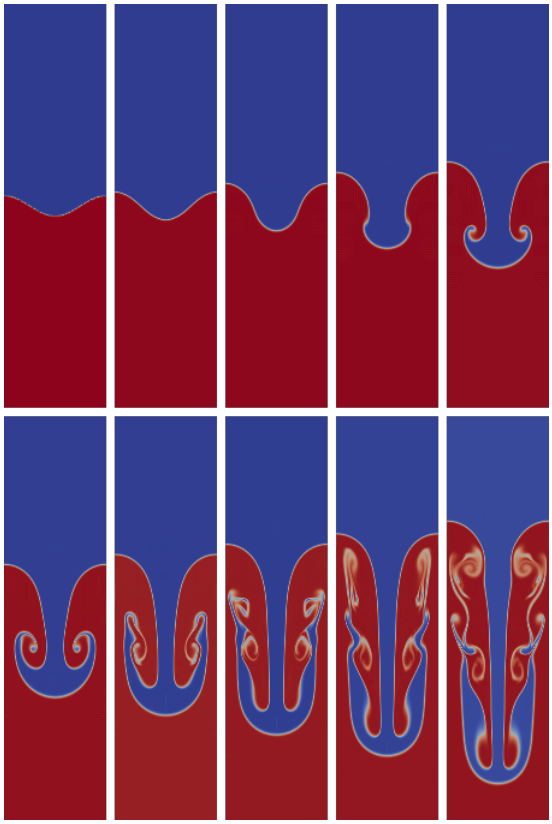

Fig. 1: The evolution of a single wavelength initial condition in the Rayleigh-Taylor instability simulation. Snapshots refer to times $t \in \{0, 0.17, 0.33, 0.5, 0.67, 0.83, 1, 1.17, 1.33, 1.5\}$ from top left to bottom right.

The analysis is finally concluded with the examination of the interface structure at a randomly selected fixed time $t = 0.79031$. As shown in Figure 3, the results are mesh and time converged for three consecutive mesh refinement levels $h \in \{2^{-5}, 2^{-6}, 2^{-7}\}$ and time step sizes $\Delta t \in \{0.004, 0.002, 0.001\}$, respectively. The main difference between the figures is in the level of detail of the vortices. Besides, the y-coordinates of the tip of the rising and falling fluids slightly differ from one mesh refinement level to the other and are thus regarded as weakly resolution dependent. Apart from that no significant differences can be observed.

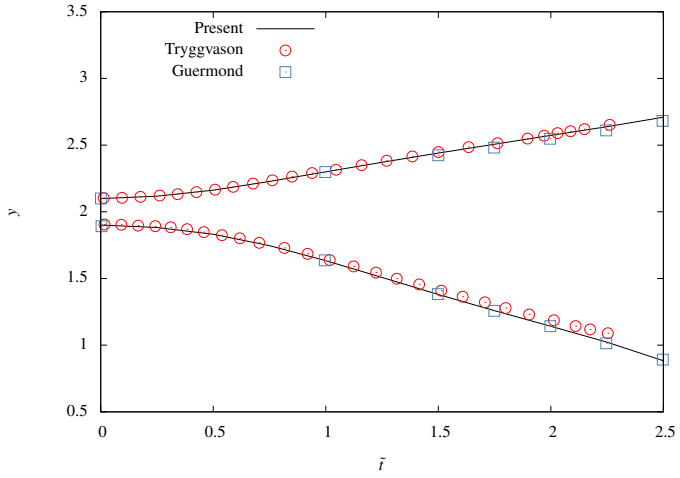

Fig. 2: The y-coordinate of the tip of the rising and falling fluid versus time.

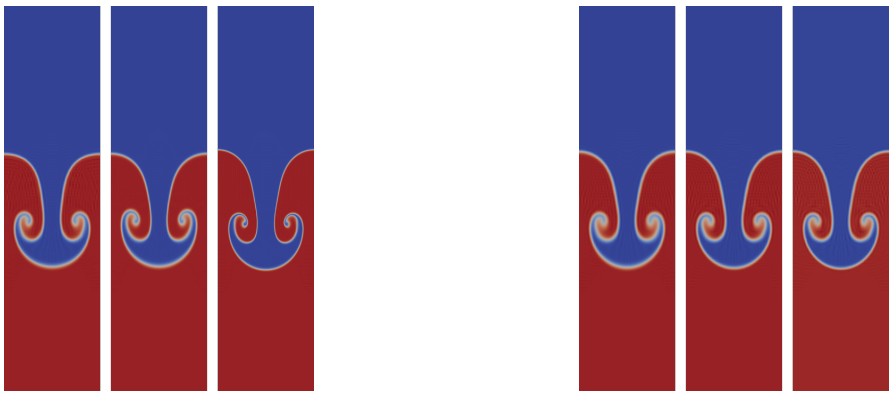

Fig. 3: Rayleigh-Taylor instability simulation at time $t = 0.79031$ with $\theta = 1, D = 0.00004, \hat{\sigma} = 0.01$. Left: Mesh converged results for $\Delta t = 0.0035, (h = 2^{-5}, \varepsilon = 0.02), (h = 2^{-6}, \varepsilon = 0.01), (h = 2^{-7}, \varepsilon = 0.005)$. Right: Time converged results for $\Delta t \in \{0.004, 0.002, 0.001\}, h = 2^{-5}, \varepsilon = 0.02$.

5 Summary and conclusions

We presented a phase field-based computational model for immiscible and incompressible two-component liquid flows based on the incompressible Navier–Stokes–Cahn–Hilliard equations. The Cahn–Hilliard equation was reformulated so as to introduce the chemical potential as an additional unknown handled by an extra equa-

tion. A weak formulation of the complex-fluid problem together with a derivation of its analytical Jacobian were presented providing enough information for hassle-free reproducibility of this work. Numerical results were presented for the Rayleigh-Taylor instability flow problem, based on Isogeometric finite element analysis of the weak formulation of the NSCH problem. The Rayleigh-Taylor instability problem has become a popular test case for numerical methods intended to study multiphase or multimaterial problems. Using the setup and reference results of Tryggvason [10] and Guermond et al. [3], we analyzed the evolution of a single wavelength interface perturbation. Qualitative comparisons of the interface shapes and quantitative analysis of the positions of the tip of the rising and falling fluid rendered our approximations to be in good correlation with the above references. Moreover, we showed our results to be mesh converged, since the produced data associated with different mesh resolutions are well comparable except for the high resolution features such as the roll-up spirals emerging at higher mesh refinement levels.

References

[1] V. E. Badalassi, H. D. Ceniceros, and S. Banerjee. Computation of multiphase systems with phase field models. *Journal of Computational Physics*, 190(2):371 – 397, 2003.

[2] H. Ding, P. D. M. Spelt, and C. Shu. Diffuse interface model for incompressible two-phase flows with large density ratios. *Journal of Computational Physics*, 226(2):2078 – 2095, 2007.

[3] J.-L. Guermond and L. Quartapelle. A projection FEM for variable density incompressible flows. *Journal of Computational Physics*, 165(1):167 – 188, 2000.

[4] M. E. Gurtin, D. Polignone, and J. Vinals. Two-phase binary fluids and immiscible fluids described by an order parameter. *Mathematical Models and Methods in Applied Sciences*, 6(6):815–831, 1996.

[5] C. W. Hirt and B. D. Nichols. Volume of fluid (VOF) method for the dynamics of free boundaries. *Journal of Computational Physics*, 39(1):201 – 225, 1981.

[6] P. C. Hohenberg and B. I. Halperin. Theory of dynamic critical phenomena. *Reviews of Modern Physics*, 49:435–479, Jul 1977.

[7] B. S. Hosseini, M. Möller, and S. Turek. Isogeometric Analysis of the Navier-Stokes equations with Taylor-Hood B-spline elements. *Applied Mathematics and Computation*, 267:264–281, 2015.

[8] J. A. Sethian. *Level Set Methods and Fast Marching Methods: Evolving Interfaces in Computational Geometry, Fluid Mechanics, Computer Vision, and Materials Science*. Cambridge Monographs on Applied and Computational Mathematics. Cambridge University Press, 1999.

[9] Y. Sun and C. Beckermann. Sharp interface tracking using the phase-field equation. *Journal of Computational Physics*, 220(2):626–653, January 2007.

[10] G. Tryggvason. Numerical simulations of the Rayleigh-Taylor instability. *Journal of Computational Physics*, 75(2):253–282, April 1988.